

# Soliton enhancement of spontaneous symmetry breaking

ALESSANDRO ALBERUCCI,<sup>1,2</sup> ARMANDO PICCARDI,<sup>1</sup> NINA KRAVETS,<sup>1</sup> OLEKSANDR BUCHNEV,<sup>3</sup> AND GAETANO ASSANTO<sup>1,2,\*</sup>

<sup>1</sup>NooEL—Nonlinear Optics and OptoElectronics Lab, University “Roma Tre”, I-00146 Rome, Italy

<sup>2</sup>Optics Laboratory, Tampere University of Technology, FI-33101 Tampere, Finland

<sup>3</sup>Optoelectronics Research Center, University of Southampton, Southampton SO17 1BJ, UK

\*Corresponding author: [assanto@uniroma3.it](mailto:assanto@uniroma3.it)

Received 29 June 2015; revised 7 August 2015; accepted 11 August 2015 (Doc. ID 243880); published 31 August 2015

**Spontaneous symmetry breaking (SSB) occurs when noise triggers an initially symmetric system to evolve toward one of its nonsymmetric states. Topological and optical SSB involve material reconfiguration/transition and light propagation/distribution in time or space, respectively. In anisotropic optical media, light beam propagation and distribution of the optic axis can be linked, thereby connecting topological and optical SSB. Using nonlinear soft matter, namely uniaxial liquid crystals, we report on simultaneous topological and optical SSB, showing that spatial solitons enhance the noise-driven transition of the medium from a symmetric to an asymmetric configuration, while acquiring a power-dependent transverse velocity in either of two specular directions with respect to the initial wavevector. Solitons enhance SSB by further distorting the optic axis distribution through nonlinear reorientation, resulting in power-tunable walk-off as well as hysteresis in beam refraction versus angle of incidence.** ©2015 Optical Society of America

**OCIS codes:** (190.6135) Spatial solitons; (190.5940) Self-action effects; (190.4420) Nonlinear optics, transverse effects in; (160.3710) Liquid crystals; (190.1450) Bistability; (190.3100) Instabilities and chaos.

<http://dx.doi.org/10.1364/OPTICA.2.000783>

## 1. INTRODUCTION

Spontaneous symmetry breaking (SSB) is known in physics, e.g., during phase transitions in matter, each of them related with a different symmetry. Topological SSB occurs in symmetrically arranged soft matter; in particular, it can affect the director distribution of nematic liquid crystals under quasi-static electric or magnetic fields [1–5], driving the generation of defects [6]. Optical SSB has been investigated in the framework of the nonlinear Schrödinger equation (NLSE), where nonlinearity is a macroscopic description of the underlying many-body physics (see, e.g., Ref. [7] and references therein). In addition to various theoretical studies and predictions, including directional couplers [8,9], (1 + 1)D and (2 + 1)D solitons [10–12], and Bragg gratings with defects [13], SSB’s destabilizing effect has been observed experimentally on temporal pulses in planar waveguides [14], on beam profiles in a photonic lattice [15], and in passive ([16,17], and references therein) as well as active resonators [18–21].

Here we introduce a novel manifestation of optical and topological SSB in a passive system, based on nonlinear optics of anisotropic soft matter: SSB determines both the final configuration of the dielectric and the direction of propagation of a self-confined light beam. An axisymmetric and bell-shaped beam initially propagates along the optic axis of a homogeneous uniaxial; noise

triggered SSB of the left/right parity results in a distortion of the medium accompanied by beam propagation in either of two (equivalent but opposite) energy-flow directions (i.e., transverse velocities) at the walk-off angle. In the self-focusing highly nonlinear regime, the beam self-confines into a spatial soliton, which in turn enhances the distortion of the nonlinear medium and determines the size of its own power-dependent walk-off, the latter limited by the birefringence. We illustrate this combined optical/topological SSB in nematic liquid crystals, i.e., uniaxial soft matter with a giant self-focusing nonlinear response that supports stable spatial solitons. In the highly nonlinear regime we model solitons accompanied by power-tunable walk-off and demonstrate for the first time, to the best of our knowledge, the soliton enhancement of SSB in this material system, presenting model, numerical simulations and experimental results. In addition, we demonstrate experimentally that the non-local self-focusing character of the material further enables a novel type of optical hysteresis in beam refraction versus angle of incidence.

## 2. OPTICAL SSB IN A UNIAXIAL MEDIUM

The propagation of light beams in anisotropic media depends on the wavevector direction and the polarization of the

electromagnetic wavepacket. In uniaxials, the anisotropy affects extraordinary eigenwaves ( $e$ -waves), resulting in a refractive index  $n_e$  that varies with the propagation direction (wavevector or phase velocity) and an energy flow (Poynting vector or group velocity in space) that is noncollinear with the latter. The angular departure of the group velocity from the phase velocity of an  $e$ -wave is known as walk-off  $\delta$  [Fig. 1(a)]. Naming  $\epsilon_{\perp}$  and  $\epsilon_{\parallel}$  the dielectric permittivities for (optical frequency) electric fields normal and parallel to the optic axis  $\hat{n}$ , respectively, if  $\theta$  is the angle between  $\hat{n}$  and the wavevector  $\mathbf{k}$ , then  $n_e = (\cos^2 \theta / \epsilon_{\perp} + \sin^2 \theta / \epsilon_{\parallel})^{-1/2}$  and  $\delta = \arctan[\epsilon_a \sin(2\theta) / (\epsilon_a + 2\epsilon_{\perp} + \epsilon_a \cos(2\theta))]$ , with  $\epsilon_a = \epsilon_{\parallel} - \epsilon_{\perp}$  the optical anisotropy. It is apparent that  $n_e(-\theta) = n_e(\theta)$  and  $\delta(-\theta) = -\delta(\theta)$ , i.e., mirror symmetry applies to light propagation. The phenomena we address in this work encompass a homogeneous distribution of the dielectric tensor, with optic axis along the input wavevector  $\mathbf{k} \parallel \hat{z}$  of a linearly polarized light beam with even profile, resulting in  $\theta = 0$  everywhere [see Fig. 1(b)]: left–right symmetry is satisfied and light propagates (as in isotropic media) with phase velocity  $c/n_o$  and  $n_o = n_{\perp} = \sqrt{\epsilon_{\perp}}$ . In a medium with a Kerr-like optical response, as the wavepacket power/intensity increases, the nonlinear polarization tends to modify the orientation of the optic axis [22,23], with positive or negative changes in  $\theta$  (hence in  $\delta$ ) being energetically equivalent and determined in sign by noise and in size by the nonlinear distortion caused by the beam: due to SSB the initially symmetric system (medium *and* beam) can spontaneously precipitate in either of two mirror-symmetric states about the  $z$  axis, breaking the left–right parity and assuming an asymmetric distribution of the optic axis with the beam traveling either upward ( $y < 0$ ) or downward ( $y > 0$ ) [Fig. 1(c)]. In self-focusing media the formation of spatial solitons via self-trapping enhances the local intensity and results in light-induced waveguides along angles adjusted by the input power [24].

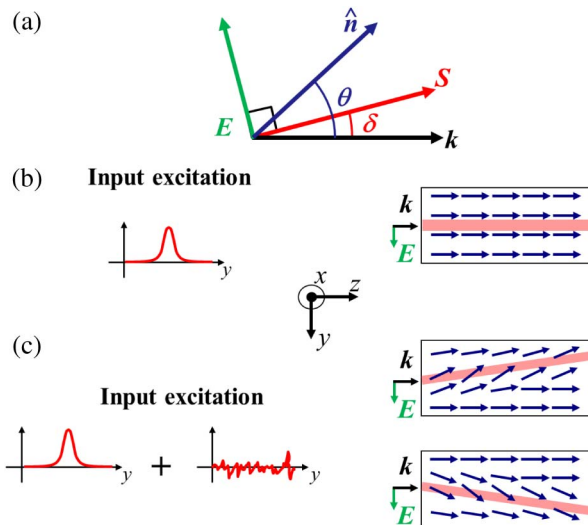


**Fig. 1.** Soliton-enhanced spontaneous symmetry breaking in uniaxials. (a) Geometry of relevant quantities in a uniaxial medium supporting spatial solitons: wavevector  $\mathbf{k}$  (taken parallel to  $\hat{z}$ ) at angle  $\theta$  with the optic axis  $\hat{n}$ , electric field  $\mathbf{E}$ , and Poynting vector  $\mathbf{S}$  at angle  $\delta$  with  $\mathbf{k}$ . (b) Parity-conserving beam propagation in the absence of noise. (c) Parity breaking due to reorientation of the optic axis in the presence of input noise and propagation of spatial solitons with walk-off.

## A. Nematic Liquid Crystals: Sample and Model

In order to observe soliton-enhanced SSB in both the material (orientation of the optic axis) and the transverse velocity of the beam as described above, the nonlinear medium has to possess two main features: a large optical anisotropy leading to an appreciable walk-off and a high all-optical response in order to access the nonperturbative nonlinear regime and give rise to spatial solitons at modest powers. An excellent candidate to this extent is nematic liquid crystals (NLCs), organic soft matter in a state with the elongated molecules randomly distributed in position but statistically aligned in a specific direction (the *molecular director*) coincident with the optic axis of the macroscopic uniaxial, typically with  $\epsilon_a > 0.5$  in the visible/near-infrared. NLCs have been widely investigated in the last few decades owing to tunability under external stimuli, low dielectric permittivity, and wide transparency [23]. Their nonlinear reorientational response stems from dipole excitation and subsequent molecule rotation in the presence of an intense electric field  $\mathbf{E}$ , as the induced torque  $\propto \epsilon_a (\hat{n} \cdot \mathbf{E})(\hat{n} \times \mathbf{E})$  acts on the director distribution and against the elastic (intermolecular) forces to minimize the overall system energy. When field  $\mathbf{E}$  of the beam and director  $\hat{n}$  are orthogonal to one another, NLCs are subject to the optical Fréedericksz transition (OFT) [25], and all-optical reorientation can only occur above a threshold excitation, with equal probability that the optic axis rotates clockwise or counterclockwise with respect to its initial alignment because of symmetry [1]. Thus, the sign of director rotation at threshold is determined by electromagnetic noise as well as thermal fluctuations, imperfections, or asymmetries, enabling SSB. Additionally, director rotations are associated with changes in the local refractive index: intense bell-shaped  $e$ -wave beams undergo self-focusing as the refractive index  $n_e$  increases with power, giving rise to self-lenses [26] and graded-index waveguides supporting spatial solitons or *nematicons* [27,28]. Beam self-trapping with low-power beams in NLCs has been widely explored [28], as the elastic interactions provide a reorientation nonlinearity with a highly nonlocal character, which, in turn, yields stable solitons even in two transverse dimensions [29,30].

In the experiments we employed a standard planar NLC cell; consistently, in the following we refer to the basic configuration in Fig. 1. The input beam is a single-hump Gaussian, linearly polarized along  $\hat{y}$  with wavevector  $\mathbf{k}$  parallel to  $\hat{z}$ . In the absence of external excitations the molecular director is homogeneously oriented along  $z$  as well, i.e.,  $\theta = 0$  everywhere. For nonzero  $\theta$  in the plane  $yz$ , beam self-trapping into *nematicons* as well as self-steering have been reported [28]. In the limit  $\theta = 0$  that we consider here, conversely, light-induced reorientation is inhibited at small powers due to the OFT [1,25]. Thus, nonlinear effects occur in a nonperturbative regime [26], in which the walk-off  $\delta$  also depends on input power and so does the beam trajectory [24]. For a proper treatment of the strong nonlinear response we write the (transverse) electric field of the  $e$ -wave beam as  $\mathbf{E}_t = \hat{t}(z)A(x, y, z)e^{ik_0 n_{\perp} z}$ , with  $k_0$  the vacuum wavenumber,  $A$  the slowly varying envelope, and  $\hat{t}(z) = \hat{y} \cos \delta(z) - \hat{z} \sin \delta(z)$  the pointwise unit vector normal to the energy flux. The electric field also possesses a longitudinal component  $\mathbf{E}_s = \hat{s}(z) \frac{i n_e \cos^2 \delta}{k_0 \epsilon_{zz}} \partial_y A$  (with  $\epsilon_{zz} = \epsilon_{\perp} + \epsilon_a \cos^2 \theta_m$ ) to consider in configurations subject to the OFT, where the subscript  $m$  refers to values at the intensity peak [22]; the subscript  $s$  indicates the direction  $\hat{s} = \hat{y} \sin \delta(z) + \hat{z} \cos \delta(z)$  of the real part of the complex Poynting vector  $\mathbf{S} = \frac{1}{2} \mathbf{E} \times \mathbf{H}^*$ . Considering a monochromatic

beam excitation in the stationary regime and defining the (rotated frame) coordinates  $x' = x$ ,  $y' = y - \tan(\delta)z$ ,  $z' = z$ , nonlinear propagation is governed by [22]

$$\frac{\partial^2 A}{\partial z'^2} + 2ik_0 n_{\perp} \frac{\partial A}{\partial z'} + \frac{\partial^2 A}{\partial x'^2} + D_y \frac{\partial^2 A}{\partial y'^2} + k_0^2 \Delta n_e^2(\theta) A = 0, \quad (1)$$

$$\begin{aligned} \nabla^2 \theta + \gamma \sin[2(\theta - \delta)](|A|^2 - |E_s|^2) \\ + 2\gamma \cos[2(\theta - \delta)]\text{Re}(\mathbf{E}_t \mathbf{E}_s^*) = 0, \end{aligned} \quad (2)$$

where  $\Delta n_e^2(\theta) = n_e^2(\theta) - n_e^2$  is the nonlinear change of the extraordinary index,  $\gamma = \epsilon_0 \epsilon_a / (4K)$  quantifies light–matter coupling ( $K$  is an effective elastic constant [23]), and  $D_y = n_e^2(\theta_m) / \epsilon_{zz}$  is the diffraction coefficient in the  $yz$  plane (differing from unity due to the anisotropy).

A direct inspection of Eqs. (1) and (2) confirms that the solutions are unaffected by the transformation  $\theta \rightarrow -\theta$ , with  $\delta(-\theta) = -\delta(\theta)$  yielding specular trajectories with respect to  $\hat{z}$  in the plane  $yz$ . As the beam power increases and overcomes the OFT, reorientation can produce a change in  $\theta$  either clockwise or counterclockwise: the initial left/right symmetry of the director distribution is determined in sign by electromagnetic and thermal noise, as well as by unavoidable imperfections in the molecular distribution/alignment. Once  $\theta \neq 0$ , beam self-focusing takes place yielding spatial solitons that propagate in the uniaxial at the corresponding walk-off, the latter upper limited by the medium anisotropy but locally determined by the soliton power through  $\theta$  [24]. The topological SSB yields a final material configuration (optic axis distribution) linked to optical SSB through beam walk-off, with transverse velocity determined in sign (positive or negative walk-off in  $yz$ ) by noise and in size by the soliton power. The nonlinear beam provides a means to observe the acquired topological asymmetry [Fig. 1(c)] and effectively increases reorientation well beyond noise levels, thereby enhancing both matter and light manifestations of SSB in the system.

### 3. SIMULATIONS AND PREDICTIONS

Equations (1) and (2) yield shape-preserving solitary wave solutions with a flat phase profile in the plane  $xy$  (i.e., normal to the wavevector along  $z$ ) and energy flux along  $\hat{s}$ . Since the full three-dimensional (2 + 1)D model [Eqs. (1) and (2)] is computationally demanding, we resorted to a simplified model retaining all the features essential to analyze SSB in anisotropic uniaxials. We simulated nonlinear light propagation using a (1 + 1)D model and the beam propagation method (BPM), addressing the role of the boundaries and accounting for strong anchoring at the cell interfaces. Since beyond OFT the beam essentially evolves in the plane  $yz$  as dictated by the input polarization and the NLC orientation, in Eq. (1) we could neglect the derivatives along  $x$ . For the reorientational Eq. (2) in (1 + 1)D we had to keep the same non-locality range of the original system, the latter range depending on the cell geometry [31]. To this extent we added a Yukawa-like term with a screening length equal to the thickness  $L_x$  across  $x$ ; the resulting equation ruling nonlinear reorientation becomes

$$\begin{aligned} \nabla_{yz}^2 \theta - \left(\frac{\pi}{L_x}\right)^2 \theta + \gamma \sin[2(\theta - \delta)](|A|^2 - |E_s|^2) \\ + 2\gamma \cos[2(\theta - \delta)]\text{Re}(\mathbf{E}_t \mathbf{E}_s^*) = 0, \end{aligned} \quad (3)$$

where the second term on the LHS is the effective screening. Consistently with the actual NLC cell used in the experiments,

we assumed the orientation angle  $\theta$  to be zero at both input ( $z = 0$ ) and output facets ( $z = 1$  mm). We launched input beams with profiles corresponding to shape-preserving solitary waves in infinitely extended samples (see Supplement 1, Section S3). Figure 2 shows the results for three excitation values  $\mathcal{P}$ , with  $\mathcal{P}$  the equivalent (1D) density power. At low powers, diffractive spreading dominates the beam dynamics in propagation along the symmetry axis  $z$ . In the case of a beam with  $\mathcal{P} = 0.81$  Wmm<sup>-1</sup> [Fig. 2(a)], appreciable reorientation takes place close to the input interface, but it cannot ensure self-confinement for large  $z$ . At higher powers, self-trapping gives rise to breathing solitons propagating with either positive ( $y > 0$ ) or negative ( $y < 0$ ) transverse velocities depending on noise realizations, consistently with SSB for  $\mathcal{P} = 0.99$  [Fig. 2(b)] and  $\mathcal{P} = 2.95$  Wmm<sup>-1</sup> [Fig. 2(c)]. Figure 3 summarizes various beam properties versus power and propagation distance. Figure 3(a) indicates an abrupt transition in reorientation between  $\mathcal{P} = 0.8$  and  $\mathcal{P} = 1.0$  Wmm<sup>-1</sup>, confirming that the OFT is first-order because of self-focusing [32,33] (see Supplement 1). Figure 3(b) shows the power-dependent trajectories, whereas Fig. 3(c) (blue line) illustrates the monotonic trend of the transverse velocity (hence output position) of the beam versus power  $\mathcal{P}$  once parity symmetry is broken (with  $|\theta_m| > 45^\circ$  after OFT [31]).

The smoking gun of SSB is the appearance of (at least) two specular local minima in the overall system energy (lightwave and NLC elastic deformation), each corresponding to broken system symmetry. A classic example is the so-called Mexican-hat potential [34]. Following Landau's standard approach to phase transitions and applying it to molecular director dynamics in liquid crystals [32], the free energy of the whole system versus  $\theta_m = \max(|\theta|)\text{sgn}(\theta)$  reads

$$\begin{aligned} F = \frac{\alpha \kappa^2 \theta_m^2}{2} + \frac{n_{\perp} P}{2c} - \frac{n_e^2(\theta_m) P}{2c n_{\perp}} \\ + \frac{\gamma Z_0 \sin[2(\theta_m - \delta_m)]}{4\pi c n_{\perp} \cos^2 \delta_m} \frac{dn_e}{d\theta} \Big|_{\theta_m} P^2 + \frac{2P}{ck_0^2 w_{\text{sol}}^2}, \end{aligned} \quad (4)$$

where  $P$  and  $w_s$  are beam power and width, respectively, and  $Z_0$  is the impedance of vacuum. The product  $\alpha \kappa^2$  depends on the soliton width  $w_{\text{sol}}$  (thus on  $\theta_m$ ), on the material, and on the geometry (as detailed in Supplement 1, Section S4). The first term in Eq. (4) stems from the elastic energy, a contribution independent

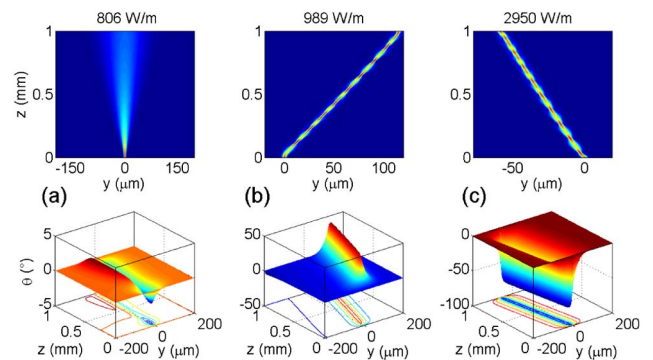


**Fig. 2.** Simulated soliton-enhanced SSB. Realizations of beam evolution in  $yz$  (upper panels) and corresponding NLC director distribution (lower graphs); the legends above indicate the input power densities. Stochastic white noise was added to the initial molecular distribution in order to initiate director motion.

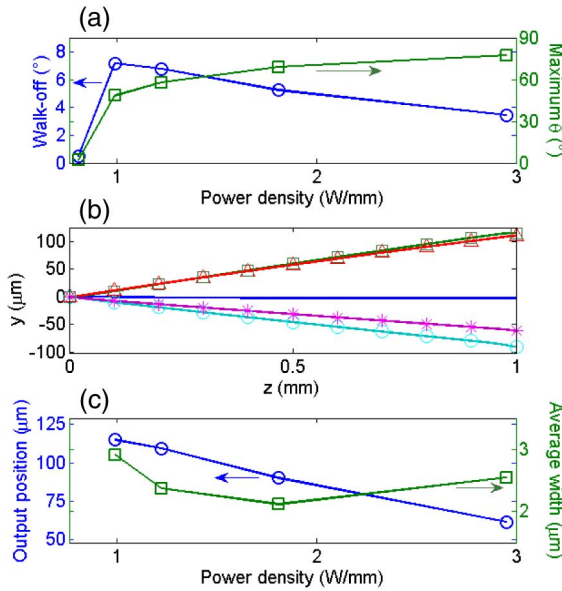


**Fig. 3.** Synopsis of nonlinear beam properties. (a) Absolute value of maximum soliton walk-off and orientation  $\theta$  versus power density. (b) Beam trajectories corresponding to the five powers marked by symbols in (a):  $0.8 \text{ Wmm}^{-1}$  (blue line without symbols),  $1.0 \text{ Wmm}^{-1}$  (green line with squares),  $1.2 \text{ Wmm}^{-1}$  (red with triangles),  $1.8 \text{ Wmm}^{-1}$  (cyan with circles), and  $2.9 \text{ Wmm}^{-1}$  (magenta with crosses). (c) Absolute output displacement across  $y$  (line with circles) and  $z$ -averaged width (line with squares) of the beam versus power density.

from beam power. The second and third terms in Eq. (4) originate from light–matter coupling in the limit of infinitely narrow beams, whereas the fourth term accounts for the finite width of the soliton. The last term proportional to  $w_{\text{sol}}^{-2}$  imposes a lower bound on soliton width owing to diffraction.

The nonlinear propagation of an  $e$ -wave light beam can be investigated by computing Eq. (4) for a given input power. For low input powers the system energy exhibits a minimum in  $\theta_m = 0$ ; i.e., no reorientation occurs because the OFT is not overcome (Fig. 4). For larger powers two absolute minima appear, symmetrically located with respect to  $\theta_m = 0$ : the overall energy landscape in Fig. 4 resembles the “sombbrero” (Mexican-hat) shape.

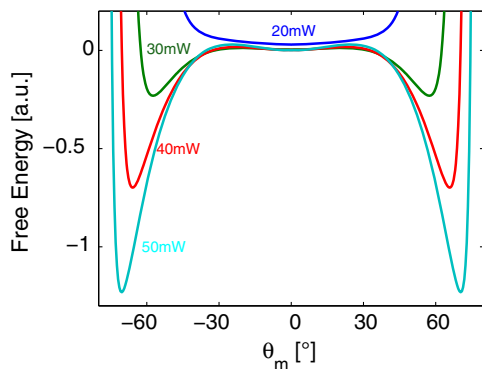


**Fig. 4.** Calculated free energy for four input powers (legends) versus reorientation angle  $\theta_m$  at the intensity peak. Oriented states are energetically favored for input powers above 20 mW.

### 4. EXPERIMENTAL RESULTS AND DISCUSSION

To experimentally confirm the theoretical analysis, we prepared a planar sample filled with the commercial E7 NLC and launched  $y$ -polarized ( $e$ -wave) fundamental Gaussian beams at  $\lambda = 1.064 \text{ }\mu\text{m}$ . First we characterized the sample using input beams slightly tilted at incidence angles  $\beta$  with respect to  $z$ . At small  $\beta$  and for sufficient powers the beams reoriented the optic axis and underwent negative refraction (i.e., when launched in  $y = 0$  its transverse velocity changed sign [35]; see Fig. 5) as well as self-confinement into spatial solitons. The beam paths in Fig. 5 demonstrate the left/right symmetry of the system (with respect to  $y = 0$ ) as the incidence angle  $\beta$  was tuned from negative to positive values.

At normal incidence ( $\beta = 0$ ) reorientation took place at powers  $P > 30 \text{ mW}$ , a threshold higher than the theoretical value due to scattering losses and longitudinal beam dynamics. Above OFT we observed SSB of the beam evolution (transverse velocity in  $yz$ ), with results markedly dependent on the point of incidence due to unavoidable errors in setting  $\beta = 0$ , beam astigmatism, imperfect NLC alignment, nonuniform anchoring across the input interface, sample inhomogeneities, NLC disclinations, and defects. Such deterministic errors dominated over noise of electromagnetic and thermal origins, as is usually the case in soft matter [5]. Moreover, as the power excitation approached the OFT threshold, i.e., close to the homogeneous/inhomogeneous phase transition associated with SSB, noise fluctuations showed a tendency to diverge, with an increase in correlation length and the formation of unequal orientation domains (opposite  $\theta$ , as in Fig. 2 bottom graphs), similar to Weiss domains in ferromagnetic media (see Supplement 1, Section S2). Correspondingly, despite the long response time of the reorientational nonlinearity, near the Fréedericksz transition we observed critical slowing down, in analogy to earlier reports of order/disorder transitions in photorefractives [36].

To experimentally assess soliton-enhanced SSB we have to reveal the presence of the two  $z$ -symmetric free energy minima at normal incidence (Fig. 4), overcoming the deterministic bias. This was accomplished by seeding the system, as illustrated in Fig. 6(a). A slight tilt  $\beta$  of the input wavevector enabled us to overcome OFT without instabilities, launching the beam with a small transverse velocity. Then, the excitation was increased

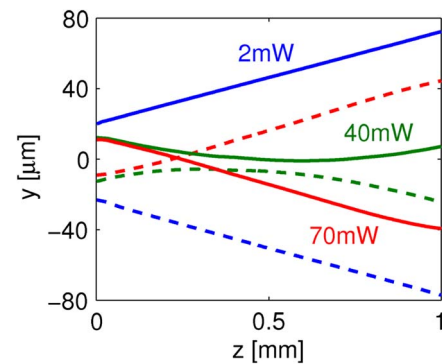


**Fig. 5.** Measured refraction of the nonlinear beam. Acquired beam trajectories at various powers for positive ( $\beta = 3^\circ$ , solid lines) and negative ( $\beta = -3^\circ$ , dashed lines) input tilts. The cases of 40 and 70 mW correspond to power-driven negative refraction. The optical wavelength is  $1.064 \text{ }\mu\text{m}$ , and the medium is the nematic E7.

until negative refraction occurred via power-dependent walk-off (see Fig. 5) [35]: the orientation  $\theta$  was in the proximity of one of the two absolute energy minima in Fig. 4. Once the beam wavevector was brought back to  $\beta = 0$  (corresponding to  $\mathbf{k} \parallel \hat{z}$ ), the refracted nonlinear beam kept track of its past whereabouts, remaining near the minimum corresponding to the previous (re)orientation  $\theta$ . Thanks to the (initial) symmetry of the system the procedure held equally well for both negative and positive  $\beta$  [see Fig. 6(a)], with two stable mirror states (opposite  $\theta$  and Poynting vector directions in the plane  $yz$ ) available at the same excitation, in agreement with SSB. Otherwise stated, (deterministic) wavevector deflections allowed us to mimic the role of (stochastic) noise while probing the existence of a pitchfork bifurcation in the system.

Figures 6(b)–6(d) show typical experimental results for normal incidence of the input beam. A beam of power  $P = 2$  mW, well below the OFT, was launched along  $z$  and propagated straight while diffracting [see Fig. 6(c)]. Then the input wavevector was slightly deflected and the power increased above OFT well into the self-trapping regime, forming a soliton; after relaxation the beam was moved back to normal incidence at the same power. Two stable states could be observed for the same excitation, as in Figs. 6(b) and 6(d): the nonlinear beam propagated with either negative [Fig. 6(b)] or positive [Fig. 6(d)] (walk-off) angles in  $yz$ , the actual sign of its direction being dictated by the sign of the previous input tilt, i.e., according to its own earlier evolution. Consistently with this highly nonlinear regime, Fig. 6(e) shows power-dependent beam trajectories (Poynting vectors), with two mirror-symmetric stable states with respect to  $y = 0$  at each power, corresponding to the two energy minima in Fig. 4.

Since  $e$ -wave nonlinear beams propagate in a system with broken symmetry according to their previous evolution (self-confinement and refraction), such memory effect can be expected to lead to hysteresis and bistability [33,37]. To this extent we explored beam dynamics for powers above OFT as the incidence angle was continuously varied along a close loop. We started with a self-deflected spatial soliton excited at negative incidence  $\beta < 0$ , thus propagating with positive walk-off and subject to negative refraction (point *a* in Fig. 7). From this state,  $\beta$  was gradually increased toward positive values (black dashes with squares in Fig. 7), while we measured the output beam position  $y_{\text{out}}$  at each step. The beam shifted to the right (i.e.,  $y_{\text{out}}$  increased) and, even after crossing the normal incidence limit  $\beta = 0$  (i.e.,  $\mathbf{k} \parallel \hat{z}$ ), remained in the half-plane  $y > 0$  evolving from negative to positive refraction, with  $y_{\text{out}}$  getting larger with  $\beta$ . In essence, the system was not able to escape from the local minimum of the overall free energy. When  $\beta \approx 2^\circ$  (point *b* in Fig. 7), the output position abruptly changed to negative values; i.e., the beam switched from standard to negative refraction. Further increases in  $\beta$  led to decreasing negative refraction (point *c* in Fig. 7), the latter eventually vanishing for large enough angles of incidence. The loop was then completed by decreasing  $\beta$  (red dashes with circles in Fig. 7), and the beam path followed a trend similar to the first half-cycle:  $y_{\text{out}}$  remained negative up to  $\beta \approx -2^\circ$ , where the beam switched from negative to positive  $y_{\text{out}}$  with an abrupt transition (point *d* in Fig. 7). Thus, for  $\beta$  in the range  $[-2^\circ, 2^\circ]$  the system showed bistable behavior stemming from the presence of two symmetric minima with respect to  $\theta = 0$  in the overall free energy plotted in Fig. 4, corroborating the observation of SSB as discussed above. Noteworthy, the cycle was left–right symmetric

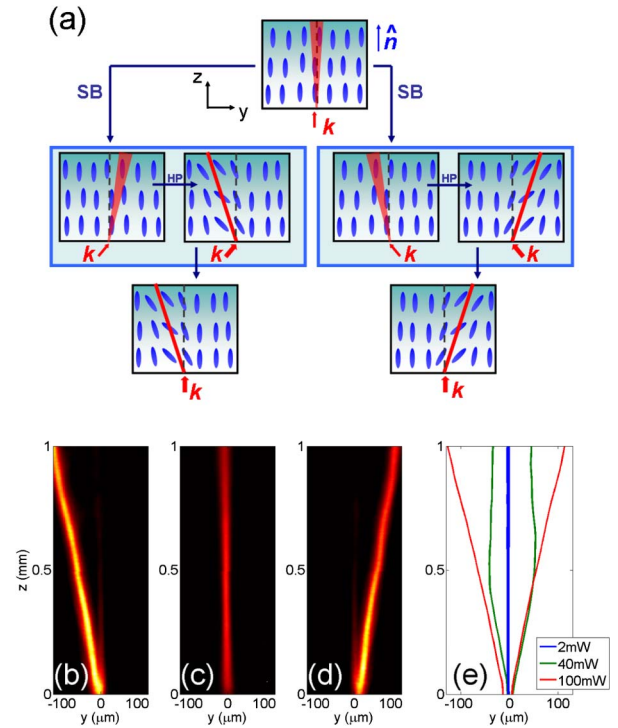


**Fig. 6.** Experimental assessment of SSB. (a) Top: the beam is incident normally to the uniform NLC with  $\theta = 0$  at powers below OFT. Center: positive and negative tilts of the input wavevector in  $y = 0$  can aid nonlinear reorientation, leading—at high enough powers (HP)—to beam self-confinement and deflection with (power-dependent) negative refraction (the transverse velocity changes sign when crossing the input interface in  $z = 0$ ). Bottom: the wavevector is brought back to normal incidence  $\mathbf{k} \parallel \hat{z}$  keeping the input power above OFT: the beam maintains/remembers self-confinement and self-deflection. The blue ellipses indicate the local alignment of the molecular director. (b)–(e) Symmetry breaking in beam propagation as the director distribution is distorted through reorientation. (b), (d) Photographs of a  $P = 100$  mW nonlinear beam undergoing (b) negative and (d) positive walk-off, respectively. (c) Linear diffraction for  $P = 2$  mW. (e) Beam trajectories for various input powers. The curved trajectories for  $P = 40$  mW (green lines) are caused by scattering losses that make optical reorientation fade away along  $z$ .

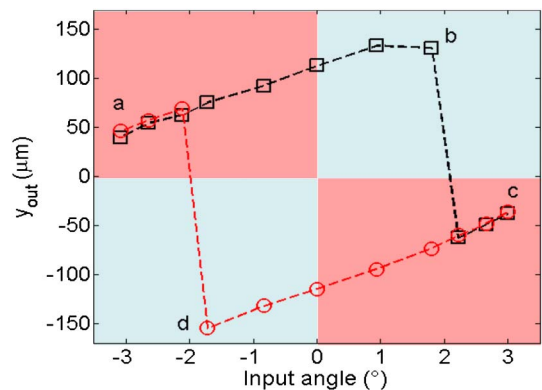


**Fig. 7.** Hysteresis of beam position versus input tilt. Output beam position  $y_{\text{out}}$  versus increasing (black squares) and decreasing (red circles) incidence angles  $\beta$  for an input power of 100 mW. The two (opposite) angles corresponding to the transitions (points *b* and *d*) depend on power. The cycle was swept clockwise from *a* to *d*. The colored areas mark positive (light blue) and negative (pink) refraction, respectively.

within experimental accuracy, thus ruling out spurious effects and artifacts due to misalignments.

## 5. CONCLUSIONS

We investigated SSB enhanced by spatial solitons in anisotropic soft matter. We specifically considered a self-focusing uniaxial dielectric initially possessing left–right symmetry: in the presence of intense and linearly polarized light beams with electric field orthogonal to the optic axis, the distribution of the latter can undergo topological SSB as the optic axis rotates either clockwise or counterclockwise, depending on noise. These two mirror states correspond to specular directions of the beam's Poynting vector in the propagation plane, i.e., opposite walk-off angles. We used NLCs, soft organic matter possessing a large reorientational response and significant anisotropy, and analyzed soliton-enhanced SSB by identifying two families of stable optical soliton solutions traveling with opposite transverse velocities, each corresponding to a distortion of the optic axis distribution with respect to the initially symmetric one. Numerical beam propagation confirmed that different noise realizations can trigger either member of the mirror-symmetric families, consistently with the two symmetric minima characterizing the free energy of the strongly coupled beam–NLC system. In the experiments with a planar cell, we verified the existence of these two states with opposite orientations  $\theta$  and corresponding walk-off angles.

In addition, we demonstrated bistability of the two mirror-symmetric beam configurations versus incidence angle, further confirming the occurrence of soliton-enhanced SSB of the medium and its manifestation through opposite transverse velocities of the beam. Our findings prove that strong light–matter coupling through nonlinear light propagation in soft matter is an ideal playground for the study of SSB and its properties, including the interplay with optical self-trapping, anisotropy, and nonlocality. Thanks to their high tunability, liquid crystals are an excellent workbench for the experimental investigation of nonlinear dynamics, including, e.g., quantum phase transitions [38].

Since spatial solitons are light-induced waveguides able to confine additional signals [27], soliton-enhanced SSB could find applications in all-optical switching, using a weak additional beam as a perturbation (seed) to trigger SSB in lieu of noise and to route the solitary waveguide (and guided signals) in either of the two specular walk-off directions determined by soliton power.

Further developments can be foreseen in the search for the equivalent of the Goldstone boson in this system [34] and in the demonstration of similar effects in nonlinear materials such as second-order parametric crystals and lattices in the cascading regime [39,40], in novel media such as the newly introduced magnetoelastic metamaterials [41], and in the study of complex SSB excitations with optical wavepackets carrying, e.g., spin and/or orbital angular momenta [42,43].

**Funding.** Suomen Akatemia (Academy of Finland) (282858).

See Supplement 1 for supporting content.

## REFERENCES

1. P. G. DeGennes and J. Prost, *The Physics of Liquid Crystals* (Oxford, 1993).
2. G. Derfel, "Field effects in nematic liquid crystals in terms of catastrophe theory," *Liq. Cryst.* **3**, 1411–1424 (1988).
3. P. E. Cladis and M. Kleman, "Non-singular disclinations," *J. Phys.* **33**, 591–598 (1972).
4. C. Williams, P. Pierański, and P. E. Cladis, "Nonsingular  $s = +1$  screw disclination lines in nematics," *Phys. Rev. Lett.* **29**, 90–92 (1972).
5. G. I. Blake, T. Mullin, and S. J. Tavener, "The Freedericksz transition as a bifurcation problem," *Dynam. Stab. Syst.* **14**, 299–331 (1999).
6. I. Chuang, R. Durrer, N. Turok, and B. Yurke, "Cosmology in the laboratory: defect dynamics in liquid crystals," *Science* **251**, 1336–1342 (1991).
7. B. A. Malomed, ed., *Spontaneous Symmetry Breaking, Self-Trapping, and Josephson Oscillation*, Progress in Optical Science and Photonics (Springer, 2013), Vol. 1.
8. A. W. Snyder, D. J. Mitchell, L. Poladian, D. R. Rowland, and Y. Chen, "Physics of nonlinear fiber couplers," *J. Opt. Soc. Am. B* **8**, 2102–2118 (1991).
9. D. A. Smirnova, A. V. Gorbach, I. V. Iorsh, I. V. Shadrivov, and Y. S. Kivshar, "Nonlinear switching with a graphene coupler," *Phys. Rev. B* **88**, 045443 (2013).
10. N. Akhmediev and A. Ankiewicz, "Novel soliton states and bifurcation phenomena in nonlinear fiber couplers," *Phys. Rev. Lett.* **70**, 2395–2398 (1993).
11. X. Shi, B. A. Malomed, F. Ye, and X. Chen, "Symmetric and asymmetric solitons in a nonlocal nonlinear coupler," *Phys. Rev. A* **85**, 053839 (2012).
12. M. Matuszewski, B. A. Malomed, and M. Trippenbach, "Spontaneous symmetry breaking of solitons trapped in a double-channel potential," *Phys. Rev. A* **75**, 063621 (2007).
13. C. M. de Sterke, I. V. Kabakova, I. Uddin, J. Jeyaratnam, and B. A. Malomed, "Spontaneous symmetry breaking in a double-defect nonlinear grating," *Phys. Rev. A* **88**, 033825 (2013).
14. C. Cambournac, T. Sylvestre, H. Maillotte, B. Vanderlinden, P. Kockaert, P. Emplit, and M. Haelterman, "Symmetry-breaking instability of multimode vector solitons," *Phys. Rev. Lett.* **89**, 083901 (2002).
15. P. Kevrekidis, Z. Chen, B. Malomed, D. Frantzeskakis, and M. Weinstein, "Spontaneous symmetry breaking in photonic lattices: theory and experiment," *Phys. Lett. A* **340**, 275–280 (2005).
16. T. Yabuzaki, T. Okamoto, M. Kitano, and T. Ogawa, "Optical bistability with symmetry breaking," *Phys. Rev. A* **29**, 1964–1972 (1984).
17. Y. Xu and S. Coen, "Experimental observation of the spontaneous breaking of the time-reversal symmetry in a synchronously pumped passive Kerr resonator," *Opt. Lett.* **39**, 3492–3495 (2014).
18. J. J. Baumberg, A. V. Kavokin, S. Christopoulos, A. J. D. Grundy, R. Butté, G. Christmann, D. D. Solnyshkov, G. Malpuech, G. Baldassarri Höger von Högersthal, E. Feltn, J.-F. Carlin, and N. Grandjean, "Spontaneous polarization buildup in a room-temperature polariton laser," *Phys. Rev. Lett.* **101**, 136409 (2008).
19. C. P. Jisha, Y. Lin, T.-D. Lee, and R.-K. Lee, "Crescent waves in optical cavities," *Phys. Rev. Lett.* **107**, 183902 (2011).
20. B. A. Malomed, "Nonlinear optics: Symmetry breaking in laser cavities," *Nat. Photonics* **9**, 287–289 (2015).
21. P. Hamel, S. Haddadi, F. Raineri, P. Monnier, G. Beaudoin, I. Sagnes, A. Levenson, and A. M. Yacomotti, "Spontaneous mirror-symmetry breaking in coupled photonic-crystal nanolasers," *Nat. Photonics* **9**, 311–315 (2015).
22. A. Alberucci and G. Assanto, "Nonparaxial solitary waves in anisotropic dielectrics," *Phys. Rev. A* **83**, 033822 (2011).
23. I. C. Khoo, "Nonlinear optics of liquid crystalline materials," *Phys. Rep.* **471**, 221–267 (2009).
24. A. Piccardi, A. Alberucci, and G. Assanto, "Soliton self-deflection via power-dependent walk-off," *Appl. Phys. Lett.* **96**, 061105 (2010).
25. S. D. Durbin, S. M. Arakelian, and Y. R. Shen, "Optical-field-induced birefringence and Freedericksz transition in a nematic liquid crystal," *Phys. Rev. Lett.* **47**, 1411–1414 (1981).
26. E. Braun, L. P. Faucheux, and A. Libchaber, "Strong self-focusing in nematic liquid crystals," *Phys. Rev. A* **48**, 611–622 (1993).
27. M. Peccianti, G. Assanto, A. D. Luca, C. Umetsu, and I. C. Khoo, "Electrically assisted self-confinement and waveguiding in planar nematic liquid crystal cells," *Appl. Phys. Lett.* **77**, 7–9 (2000).
28. M. Peccianti and G. Assanto, "Nematicons," *Phys. Rep.* **516**, 147–208 (2012).
29. A. W. Snyder and D. J. Mitchell, "Accessible solitons," *Science* **276**, 1538–1541 (1997).

30. C. Conti, M. Peccianti, and G. Assanto, "Route to nonlocality and observation of accessible solitons," *Phys. Rev. Lett.* **91**, 073901 (2003).
31. A. Alberucci, A. Piccardi, M. Peccianti, M. Kaczmarek, and G. Assanto, "Propagation of spatial optical solitons in a dielectric with adjustable nonlinearity," *Phys. Rev. A* **82**, 023806 (2010).
32. H. L. Ong, "Optically induced Freedericksz transition and bistability in a nematic liquid crystal," *Phys. Rev. A* **28**, 2393–2407 (1983).
33. N. Kravets, A. Piccardi, A. Alberucci, O. Buchnev, M. Kaczmarek, and G. Assanto, "Bistability with optical beams propagating in a reorientational medium," *Phys. Rev. Lett.* **113**, 023901 (2014).
34. J. Goldstone, "Field theories with superconductor solutions," *Il Nuovo Cimento* **19**, 154–164 (1961).
35. A. Piccardi, A. Alberucci, N. Kravets, O. Buchnev, and G. Assanto, "Power-controlled transition from standard to negative refraction in reorientational soft matter," *Nat. Commun.* **5**, 5533–5541 (2014).
36. D. Engin, S. Orlov, M. Segev, G. C. Valley, and A. Yariv, "Order-disorder phase transition and critical slowing down in photorefractive self-oscillators," *Phys. Rev. Lett.* **74**, 1743–1746 (1995).
37. J. Beeckman, A. Madani, P. J. M. Vanbrabant, P. Henneaux, S.-P. Gorza, and M. Haelterman, "Switching and intrinsic position bistability of soliton beams in chiral nematic liquid crystals," *Phys. Rev. A* **83**, 033832 (2011).
38. M. Nikkhou, M. Skarabot, S. Copar, M. Ravnik, S. Zumer, and I. Musevic, "Light-controlled topological charge in a nematic liquid crystal," *Nat. Phys.* **11**, 183–187 (2015).
39. D. Y. Kim, P. Vidakovic, W. E. Moerner, R. Twieg, J. Zyss, W. E. Torruellas, J. Kang, G. Bjorklund, C. Bosshard, and G. I. Stegeman, "Second-order cascading as the origin of large third-order effects in organic single-crystal-core fibers," *Opt. Lett.* **19**, 868–870 (1994).
40. K. Gallo, A. Pasquazi, S. Stivala, and G. Assanto, "Parametric solitons in two-dimensional lattices of purely nonlinear origin," *Phys. Rev. Lett.* **100**, 053901 (2008).
41. M. Liu, D. A. Powell, I. A. Shadrivov, M. Lapine, and Y. S. Kivshar, "Spontaneous chiral symmetry breaking in metamaterials," *Nat. Commun.* **5**, 4441 (2014).
42. R. Dorn, S. Quabis, and G. Leuchs, "Sharper focus for a radially polarized light beam," *Phys. Rev. Lett.* **91**, 233901 (2003).
43. R. Barboza, U. Bortolozzo, G. Assanto, E. Vidal-Henriquez, M. G. Clerc, and S. Residori, "Harnessing optical vortices in soft matter lattices," *Phys. Rev. Lett.* **111**, 093902 (2013).